J|A|C|S
ARTICLES
Published on Web 10/25/2002

Novel Mixed-Valent (V/VI) Triple Perovskite Ruthenates: Observation of a Complex Low-Temperature Structural and Magnetic Transition

Katharine E. Stitzer, Mark D. Smith, William R. Gemmill, and Hans-Conrad zur Loye*

Contribution from the Department of Chemistry and Biochemistry, University of South Carolina, Columbia, South Carolina 29208

Received June 5, 2002

Abstract: Two new mixed-valent triple perovskites, $Ba_3MRu_2O_9$ (M = Li, Na), were grown from reactive hydroxide fluxes. They crystallize in the hexagonal space group $P6_3/mmc$, where Ru(V) and Ru(VI) are disordered on only one crystallographic site. Upon cooling, single crystals of $Ba_3NaRu_2O_9$ undergo a complex symmetry-breaking structural transition at ca. 225 K from room-temperature hexagonal symmetry to a low-temperature orthorhombic symmetry, space group *Cmcm*. Accompanying this structural transition is a rather abrupt decrease in the magnetic susceptibility at 210 K followed by a steady decrease in the susceptibility with decreasing temperature. Interestingly, the lithium analogue does not display any structural transition down to 100 K. The structural transition in $Ba_3NaRu_2O_9$ generates three crystallographically unique Ru sites in the low-temperature structure as compared to only one distinct site in the room-temperature structure. On the basis of an analysis of the Ru−Ru distances in the face-sharing bi-octahedra, the structural transition also appears to involve charge ordering of Ru(V) and Ru(VI), causing all Ru(V) to occupy one set of bi-octahedra and all Ru(VI) to occupy another set.

Introduction

In the field of solid state chemistry, the perovskite family of oxides is perhaps the most studied group of oxides known. What has generated and sustained the interest in this fascinating family of oxides is the large and ever surprising variety of properties exhibited, as well as the compositional flexibility[1] that enables this structure to accommodate almost every element in the periodic table. Many investigations, consequently, have focused on the study of specific properties including complex magnetic phenomena and electrical properties such as superconductivity, ferroelectricity, and ionic conductivity, to mention a few, while others explored the synthesis of new compositions or the stabilization of metals in heretofore unreported or unusual oxidation states.[1−5]

In its ideal form, the structure of the cubic ABO_3 perovskite can be described as consisting of corner-sharing BO_6 octahedra with the A cation occupying the 12-fold coordination site formed in the middle of a cube of eight such octahedra, while the 2H-hexagonal variant consists of infinite chains of face-sharing octahedra that are separated by chains of the A cation. Both the cubic and the hexagonal perovskite structures can be generated from the stacking of close packed $[AO_3]$ layers and the subsequent filling of the generated octahedral sites by the B cation, where an ABC type stacking results in the cubic and an AB stacking results in the hexagonal (2H) perovskite structure.[6,7] In addition to the cubic and hexagonal ABO_3 structures, there exists a variety of intergrowth structures that combine the AB and ABC stacking sequences. Thus, the triple perovskite, $A_3BB'_2O_9$, contains both corner-sharing octahedra, consistent with ABC stacking, and face-sharing bi-octahedra, consistent with AB stacking.

Among the perovskites, the ruthenates in particular have attracted much attention due to the structural variety exhibited (simple, double, triple, and quadruple perovskite structure)[8−13] and the existence of several accessible oxidation states (+4, +5, +6, +7)[11,12,14] and the resulting interesting magnetic behaviors that have been observed.[9,13,15] The formal oxidation state(s) of the ruthenium are determined by a combination of the overall elemental composition, that is, the specific M cation,

* To whom correspondence should be addressed. E-mail: zurloye@sc.edu.

(1) Stitzer, K. E.; Darriet, J.; zur Loye, H.-C. *Curr. Opin. Solid State Mater. Sci.* **2001**, *5*, 535.
(2) Schneemeyer, L. F.; Thomas, J. K.; Siegrist, T.; Batlogg, B.; Rupp, L. W.; Opila, R. L.; Cava, R. J.; Murphy, D. W. *Nature* **1988**, *335*, 421.
(3) Kendall, K. R.; Navas, C.; Thomas, J. K.; zur Loye, H.-C. *Solid State Ionics* **1995**, *82*, 215.
(4) Stitzer, K. E.; Smith, M. D.; zur Loye, H.-C. *Solid State Sci.* **2002**, *4*, 311.
(5) Reisner, B. A.; Stacy, A. M. *J. Am. Chem. Soc.* **1998**, *120*, 9682.
(6) Lander, J. J. *Acta Crystallogr.* **1951**, *4*, 148.
(7) Wells, A. F. *Structural Inorganic Chemistry*, 5th ed.; Clarendon Press: New York, 1984.
(8) Randal, J. J.; Ward, R. *J. Am. Chem. Soc.* **1959**, *81*, 2629.
(9) Kim, S. H.; Battle, P. D. *J. Solid State Chem.* **1995**, *114*, 174.
(10) Battle, P. D.; Jones, C. W. *J. Solid State Chem.* **1989**, *78*, 108.
(11) Lightfoot, P.; Battle, P. D. *J. Solid State Chem.* **1990**, *89*, 174.
(12) Doi, Y.; Wakeshima, M.; Hinatsu, Y.; Tobo, A.; Ohoyama, K.; Yamaguchi, Y. *J. Mater. Chem.* **2001**, *11*, 3135.
(13) Battle, P. D.; Kim, S. H.; Powell, A. V. *J. Solid State Chem.* **1992**, *101*, 161.
(14) Samata, H.; Mishiro, A.; Sawada, S.; Nagata, Y.; Uchida, T.; Kai, M.; Ohtsuka, M.; Der Lan, M. *J. Phys. Chem. Solids* **1998**, *59*, 1445.
(15) Darriet, J.; Drillion, M.; Villeneuve, G.; Hagenmuller, P. *J. Solid State Chem.* **1976**, *19*, 213.

and the particular structural variant, that is, double perovskite $Ba_2M(II)Ru(VI)O_6$, triple perovskite $Ba_3M(II)Ru(V)_2O_9$, quadruple perovskite $Ba_4M(I)Ru(V)_3O_{12}$, etc. The combination of a fixed valent M element, such as alkali metals, alkaline earths and rare earths, and a specific structural variant, can give rise to mixed valency. Thus, the rare-earth-containing triple perovskite $Ba_3RE(III)Ru(IV)Ru(V)O_9$[16] results in a mixed-valent Ru(IV/V) oxide. The use of an alkali metal instead of the rare earth metal results in mixed-valent Ru(V/VI) triple perovskites $Ba_3MRu_2O_9$ (M = Li, Na), the title compounds of this paper.

For the past 10 years, our group has explored the single-crystal growth of perovskite-related oxides from high-temperature solutions.[4,17−25] More recently, we have focused our attention on ruthenium-containing oxides and on establishing the conditions by which high-quality single crystals can be grown from high-temperature solutions. This well-established method[26] is particularly applicable to oxides, as exemplified by the numerous published compositions containing elements from nearly every section of the periodic table in a wide range of oxidation states.[26] Oxide crystals have been grown from many different high-temperature solutions, including alkali and alkaline earth carbonates, halides, peroxides, super oxides, and hydroxides.[18,19,27−31] Of all of these diverse solvent systems, the hydroxide melts have proven to be particularly advantageous for obtaining single crystals containing elements in unusually high oxidation states, as exemplified by systems such as Ni(IV) in $Ba_6Ni_5O_{15}$,[32] Rh(V) in Sr_3NaRhO_6,[5] and Os(VII) in Ba_2NaOsO_6.[4] It therefore proved possible to obtain high-quality crystals of unusually high oxidation state ruthenium(V/VI) triple perovskites containing alkali metals from hydroxide melts. The growth of these crystals and their structure determination, including unexpected low-temperature structural and magnetic transitions, are detailed in this paper.

Experimental Section

Crystal Growth. RuO_2 (synthesized from heating Ru powder (Engelhard, 99.5%) in air at 1000 °C for 24 h) (0.1331 g, 1.00 mmol), $Ba(OH)_2{\cdot}8H_2O$ (1.0280 g, 3.25 mmol; Fisher, ACS reagent), and $LiOH{\cdot}H_2O$ (5.82 g, 139 mmol; Alfa Aesar, ACS reagent), with KOH (3.91 g, 69.7 mmol; Fisher, ACS reagent) for $Ba_3LiRu_2O_9$ and NaOH (11.63 g, 291 mmol; Fisher, ACS reagent) for $Ba_3NaRu_2O_9$, were placed in an alumina crucible. The filled crucibles were covered with an alumina lid and heated to the reaction temperature of 700 °C at 600 °C/h. The reactions were held at temperature for 12 h and then slowly cooled to 600 °C at 15 °C/h followed by cooling to room temperature by turning off the furnace. The flux was dissolved with water in the case of the sodium preparation and methanol for the lithium preparation. Flux dissolution was also aided by the use of sonication followed by the manual isolation of the crystals.

Although single crystals of $Ba_3LiRu_2O_9$ were isolated from the aforementioned reaction, the crystals of $Ba_3LiRu_2O_9$ were always accompanied by a small amount of an impurity phase. To prepare a single phase sample of $Ba_3LiRu_2O_9$, RuO_2 (0.1360 g, 1.02 mmol), $Ba(OH)_2{\cdot}8H_2O$ (1.0330 g, 3.28 mmol; Fisher, ACS reagent), $LiOH{\cdot}H_2O$ (5.87 g, 140 mmol; Alfa Aesar, ACS reagent) with KOH (4.09 g, 72.9 mmol; Fisher, ACS reagent), and H_2O (2.00 g, 111 mmol) were placed in an alumina crucible. The filled crucible was tightly covered with a secondary upside-down porcelain crucible and heated to the reaction temperature of 700 °C at 600 °C/h. The reaction was held at temperature for 12 h and then slowly cooled to 600 °C at 15 °C/h followed by cooling to room temperature by turning off the furnace. The flux was dissolved with methanol, aided by sonication followed by manual isolation of the crystals. Powder X-ray diffraction confirmed the sample to be phase pure $Ba_3LiRu_2O_9$. The single-crystal structure solution was carried out on the first preparation of $Ba_3LiRu_2O_9$, while the magnetic susceptibility data were collected using the second phase pure sample.

Data Collection. For the structure determination of $Ba_3LiRu_2O_9$ and $Ba_3NaRu_2O_9$, a black hexagonal needle and a black hexagonal block, respectively, were mounted onto the end of thin glass fibers. X-ray intensity data were measured at 293 K on a Bruker SMART APEX CCD-based diffractometer system (Mo Kα radiation, $\lambda = 0.71073$ Å).[33]

Crystal quality and initial hexagonal unit cell parameters were determined on the basis of reflections taken from a set of three scans measured in orthogonal regions of reciprocal space. Subsequently 1650 raw data frames were collected in ω scan mode (0.3° frame width, 20 s per frame) at three different ϕ settings for $Ba_3LiRu_2O_9$ and 1580 raw data frames (0.3° frame width in ω, 10 s per frame) at four different ϕ settings for $Ba_3NaRu_2O_9$. The collection provided 100% coverage of reciprocal space to $2\theta_{max} = 80.1°$ ($R_{int} = 0.0532$, average redundancy = 9.59) and $2\theta_{max} = 75.6°$ ($R_{int} = 0.0279$, average redundancy = 10.54) for $Ba_3LiRu_2O_9$ and $Ba_3NaRu_2O_9$, respectively. The raw data frames were integrated with Bruker SAINT+,[33] which also applied corrections for Lorentz and polarization effects. The final unit cell parameters were based on the least-squares refinement of 2926 reflections for $Ba_3LiRu_2O_9$ and 4313 reflections for $Ba_3NaRu_2O_9$ with $I > 5\sigma(I)$ from the data set. Analysis of each data set showed negligible crystal decay during data collection. An empirical absorption correction based on the multiple measurement of equivalent reflections was applied with the program SADABS.[34]

For both $Ba_3LiRu_2O_9$ and $Ba_3NaRu_2O_9$, systematic absences in the intensity data were consistent with the space group $P6_3/mmc$. The structures were solved by a combination of direct methods and difference Fourier syntheses, and refined by full-matrix least-squares against F^2, using the SHELXTL software package.[34] All atoms were refined with anisotropic displacement parameters. No significant deviation from unity occupancy was observed for any of the heavy atoms, on the basis of the refinement of the site occupation factors for those atoms. The largest residual electron density peak and hole remaining in the final difference map are +1.57 and −3.10 $e^-/Å^3$, located in the vicinity of the Ba atoms for $Ba_3LiRu_2O_9$, and +1.30 and −1.35 $e^-/Å^3$, located 0.67 and 0.82 Å from Ba2 and Ba1, respectively, for $Ba_3NaRu_2O_9$. Relevant crystallographic information is compiled in

(16) Doi, Y.; Hinatsu, Y.; Shimojo, Y.; Ishii, Y. *J. Solid State Chem.* **2001**, *161*, 113.
(17) Claridge, J. B.; Layland, R. C.; Adams, R. D.; zur Loye, H.-C. *Z. Anorg. Allg. Chem.* **1997**, *623*, 1131.
(18) Claridge, J. B.; Layland, R. C.; Henley, W. H.; zur Loye, H.-C. *Chem. Mater.* **1999**, *11*, 1376.
(19) Henley, W. H.; Claridge, J. B.; Smallwood, P. L.; zur Loye, H.-C. *J. Cryst. Growth* **1999**, *204*, 122.
(20) Smith, M. D.; zur Loye, H.-C. *Acta Crystallogr.* **2001**, *C57*, 337.
(21) Stitzer, K. E.; El Abed, A.; Darriet, J.; zur Loye, H.-C. *J. Am. Chem. Soc.* **2001**, *123*, 8790.
(22) Stitzer, K. E.; Smith, M. D.; Darriet, J.; zur Loye, H.-C. *Chem. Commun.* **2001**, 1680.
(23) zur Loye, H.-C.; Layland, R. C.; Smith, M. D.; Claridge, J. B. *J. Cryst. Growth* **2000**, *211*, 452.
(24) zur Loye, H.-C.; Stitzer, K. E.; Smith, M. D.; El Abed, A.; Darriet, J. *Inorg. Chem.* **2001**, *40*, 5152.
(25) Zakhour-Nakhl, M.; Claridge, J. B.; Darriet, J.; Weill, F.; zur Loye, H.-C.; Perez-Mato, J. M. *J. Am. Chem. Soc.* **2000**, *122*, 1618.
(26) Elwell, D.; Scheel, H. J. *Crystal Growth from High-Temperature Solutions*; Acadmeic Press: New York, 1975.
(27) Frenzen, S.; Müller-Buschbaum, H. *Z. Naturforsch.* **1995**, *50b*, 581.
(28) Neubacher, M.; Müller-Buschbaum, H. *Z. Anorg. Allg. Chem.* **1992**, *607*, 124.
(29) Smith, M. D.; Stalick, J. K.; zur Loye, H.-C. *Chem. Mater.* **1999**, *11*, 2984.
(30) Wehrum, G.; Hoppe, R. *Z. Anorg. Allg. Chem.* **1992**, *617*, 45.
(31) Stitzer, K. E.; Smith, M. D.; zur Loye, H.-C. *J. Alloys Compd.* **2002**, *338*, 104.
(32) Campá, J. A.; Gutiérrez-Puebla, E.; Monge, M. A.; Rasines, I.; Ruíz-Valero, C. *J. Solid State Chem.* **1994**, *108*, 230.
(33) *SMART Version 5.624, SAINT+ Version 6.02a and SADABS*; Bruker Analytical X-ray Systems, Inc.: Madison, WI, 1998.
(34) Sheldrick, G. M. *SHELXTL Version 5.1*; Bruker Analytical X-ray Systems, Inc.: Madison, WI, 1997.

Table 1. Crystallographic Data and Structure Refinement for $Ba_3LiRu_2O_9$

empirical formula	$Ba_3LiRu_2O_9$
formula weight	765.10
temperature	293(2) K
wavelength	0.71073 Å
crystal system	hexagonal
space group	$P6_3/mmc$
unit cell dimensions	$a = 5.7820(2)$ Å, $\alpha = 90°$ $b = 5.7820(2)$ Å, $\beta = 90°$ $c = 14.1490(8)$ Å, $\gamma = 120°$
volume	409.65(3) Å^3
Z	2
density (calculated)	6.203 Mg/m^3
absorption coefficient	17.832 mm^{-1}
reflections collected	5488
independent reflections	542 [R(int) = 0.0532]
absorption correction	semiempirical from equivalents
data/restraints/parameters	542/0/22
GOF on F^2	1.089
final R indices [$I > 2\sigma(I)$]	R1 = 0.0293, wR2 = 0.0673
R indices (all data)	R1 = 0.0368, wR2 = 0.0708
extinction coefficient	0.0139(11)
largest diff. peak and hole	1.567 and −3.103 e Å^{-3}

Table 2. Crystallographic Data and Structure Refinement for the Room-Temperature Solution of $Ba_3NaRu_2O_9$

empirical formula	$Ba_3NaRu_2O_9$
formula weight	781.15
temperature	293(2) K
wavelength	0.71073 Å
crystal system	hexagonal
space group	$P6_3/mmc$
unit cell dimensions	$a = 5.8729(2)$ Å, $\alpha = 90°$ $b = 5.8729(2)$ Å, $\beta = 90°$ $c = 14.4676(7)$ Å, $\gamma = 120°$
volume	432.15(3) Å^3
Z	2
density (calculated)	6.003 Mg/m^3
absorption coefficient	16.956 mm^{-1}
reflections collected	5370
independent reflections	492 [R(int) = 0.0279]
absorption correction	semiempirical from equivalents
data/restraints/parameters	492/0/22
GOF on F^2	1.138
final R indices [$I > 2\sigma(I)$]	R1 = 0.0213, wR2 = 0.0485
R indices (all data)	R1 = 0.0233, wR2 = 0.0494
extinction coefficient	0.0369(12)
largest diff. peak and hole	1.296 and −1.354 e Å^{-3}

Table 3. Atomic Coordinates and Equivalent Isotropic Parameters for $Ba_3LiRu_2O_9$

atom	x	y	z	U_{eq} (Å^2)
Ba(1)	1/3	2/3	0.5907(1)	0.012(1)
Ba(2)	0	0	1/4	0.009(1)
Li(1)	0	0	0	0.035(7)
Ru(1)	1/3	2/3	0.3478(1)	0.007(1)
O(1)	0.4828(4)	0.9656(8)	1/4	0.009(1)
O(2)	0.1744(3)	0.3488(6)	0.4148(2)	0.013(1)

Tables 1 and 2 for $Ba_3LiRu_2O_9$ and $Ba_3NaRu_2O_9$, respectively, and the atomic positions are located in Tables 3 and 4 for $Ba_3LiRu_2O_9$ and $Ba_3NaRu_2O_9$, respectively.

Upon completing the collection of the room-temperature data for $Ba_3NaRu_2O_9$, we mounted the same crystal onto the end of a thin glass fiber using inert oil and aligned it in the nitrogen cold stream. Beginning at 293 K, the temperature was lowered incrementally, approximately 10 K at a time. Several raw data frames were collected at each temperature and examined for indications of a structural transition. At approximately 225(2) K, the diffraction pattern changed dramatically. Although the reflections could still be indexed to a primitive hexagonal unit cell, the true symmetry was later determined to be orthorhombic (vide infra). Intensity data were measured at 173(2) K on a Bruker SMART APEX CCD-based diffractometer system (Mo Kα radiation, $\lambda = 0.71073$ Å)[33] to provide complete coverage in orthorhombic symmetry to $2\theta_{max} \approx 60°$. The raw data frames were integrated and merged according to *mmm* Laue symmetry restrictions with SAINT+.[33] The final unit cell parameters were based on the least-squares refinement of 9637 reflections from the data set with $I > 5(\sigma)I$. Analysis of the data showed negligible crystal decay during data collection. An empirical absorption correction based on the multiple measurement of equivalent reflections was applied with the program SADABS.[33]

Table 4. Atomic Coordinates and Equivalent Isotropic Parameters for the Room-Temperature Solution of $Ba_3NaRu_2O_9$

atom	x	y	z	U_{eq} (Å^2)
Ba(1)	2/3	1/3	0.0924(1)	0.017(1)
Ba(2)	0	0	1/4	0.012(1)
Na(1)	0	0	0	0.009(1)
Ru(1)	1/3	2/3	0.1550(1)	0.009(1)
O(1)	0.1778(3)	0.3556(6)	0.0899(2)	0.018(1)
O(2)	0.0354(7)	0.5177(4)	1/4	0.012(1)

Table 5. Crystallographic Data and Structure Refinement for the Low-Temperature Solution of $Ba_3NaRu_2O_9$

empirical formula	$Ba_3NaRu_2O_9$
formula weight	781.15
temperature	173(2) K
wavelength	0.71073 Å
crystal system	orthorhombic
space group	*Cmcm*
unit cell dimensions	$a = 11.7282(8)$ Å, $\alpha = 90°$ $b = 20.3541(13)$ Å, $\beta = 90°$ $c = 14.4856(10)$ Å, $\gamma = 90°$
volume	3458.0(4) Å^3
Z	16
density (calculated)	6.002 Mg/m^3
absorption coefficient	16.953 mm^{-1}
reflections collected	15 644
independent reflections	3038 [R(int) = 0.0411]
absorption correction	semiempirical from equivalents
data/restraints/parameters	3038/0/107
GOF on F^2	1.092
final R indices [$I > 2\sigma(I)$]	R1 = 0.0331, wR2 = 0.0846
R indices (all data)	R1 = 0.0377, wR2 = 0.0869
largest diff. peak and hole	2.858 and −2.302 e Å^{-3}

Because of the presence of twinning, the systematic absences in the intensity data were ambiguous, with several strong violations of the c-glide element of the space group *Cmcm*. However, the structure was readily solved in this space group by a combination of direct methods and difference Fourier syntheses and was refined by full-matrix least-squares against F^2, using the SHELXTL software package.[34] This space group choice was later verified by inspection of the structure as well as with the ADDSYM routine in PLATON.[35]

Probably because of a combination of the effects of the deterioration in crystal quality, as indicated by broadening of the diffraction spot profiles, and the twinning, only the Ba and Ru atoms could be refined with anisotropic displacement parameters; Na and O atoms were refined isotropically. At convergence, the largest difference peak and hole are +2.86 and −2.30 e$^-$/Å^3, respectively, both located <1 Å from Ba6. Relevant crystallographic information is compiled in Table 5 for the low-temperature structure solution of $Ba_3NaRu_2O_9$, and the corresponding atomic positions are located in Table 6.

A single crystal of $Ba_3LiRu_2O_9$ was similarly treated; however, no evidence of a structural phase transition was detected down to the lowest temperature measured (100 K).

(35) Spek, A. L. *PLATON, A Multipurpose Crystallographic Tool*; Utrecht University: Utrecht, The Netherlands, 1998.

Table 6. Atomic Coordinates and Equivalent Isotropic Parameters for the Low-Temperature Solution of $Ba_3NaRu_2O_9$

atom	*x*	*y*	*z*	U_{eq} (Å^2)
Ba(1)	0	0.0093(1)	3/4	0.010(1)
Ba(2)	0	0.4916(1)	1/4	0.008(1)
Ba(3)	0.2493(2)	0.2465(1)	1/4	0.009(1)
Ba(4)	1/2	0.1709(1)	0.0839(1)	0.010(1)
Ba(5)	0	0.1714(1)	0.0809(1)	0.011(1)
Ba(6)	0.2500(2)	0.9070(1)	0.0985(1)	0.010(1)
Ru(1)	1/2	0.3307(1)	0.1598(1)	0.007(1)
Ru(2)	0	0.3307(1)	0.1584(1)	0.008(1)
Ru(3)	0.2494(2)	0.0782(1)	0.1517(1)	0.008(1)
Na(1)	1/4	1/4	0	0.012(1)
Na(2)	1/2	0	0	0.020(3)
Na(3)	0	0	0	0.007(2)
O(11)	0.3758(10)	0.2911(6)	0.0921(7)	0.017(2)
O(12)	1/2	0.2503(13)	1/4	0.023(6)
O(13)	0.6210(12)	0.3644(7)	1/4	0.010(3)
O(14)	1/2	0.4110(5)	0.0915(7)	0.002(2)
O(21)	0.1125(9)	0.2925(5)	0.0890(6)	0.005(2)
O(22)	0	0.2569(9)	1/4	0.002(3)
O(23)	0	0.4032(8)	0.0812(10)	0.016(3)
O(24)	0.1159(11)	0.3720(6)	1/4	0.001(2)
O(31)	0.2472(14)	0.1537(4)	0.0809(5)	0.014(1)
O(32)	0.1441(17)	0.1178(10)	1/4	0.021(4)
O(33)	0.3559(19)	0.1158(11)	1/4	0.029(5)
O(34)	0.3468(8)	0.0351(4)	0.0778(5)	0.015(2)
O(35)	0.1121(7)	0.0507(4)	0.1088(5)	0.014(1)
O(36)	0.2447(17)	0.0060(5)	1/4	0.013(2)

Magnetic Susceptibility. The magnetic susceptibility of $Ba_3MRu_2O_9$ (M = Li, Na) was measured using a Quantum Design MPMS XL SQUID magnetometer. For the magnetic measurements, loose crystals of the ruthenates were placed into a gelatin capsule, which was placed inside a plastic straw. Samples were measured under both zero field cooled (zfc) and field cooled (fc) conditions. In either case, the magnetization was measured in the temperature range from 2 to 400 K. Susceptibility measurements were carried out in applied fields of 0.5, 1, 5, and 20 kG. The very small diamagnetic contribution of the gelatin capsule containing the sample had a negligible contribution to the overall magnetization, which was dominated by the sample signal.

High-temperature susceptibility data were collected using the Quantum Design oven attachment. Loose single crystals of $Ba_3MRu_2O_9$ (M = Li, Na) were placed inside a two-part brass sample holder. The sample holder was machined from a solid brass rod measuring 3 mm in diameter and 15 cm in length and unscrews into two pieces at the center. The sample was placed into a cavity that was machined into the lower half of the brass sample holder. Data were collected in an applied field of 20 kG in the temperature range from 300 to 650 K. The moment of the sample holder was corrected for using the Automatic Background Subtraction software supplied by Quantum Design.

Microscopy. Scanning electron micrographs of several single crystals were obtained using a Philips XL 30 ESEM instrument utilized in the environmental mode. An ESEM image of a typical crystal is shown in Figure 1. The ESEM also verified the presence of barium, ruthenium, and oxygen in all samples, and the presence of sodium in $Ba_3NaRu_2O_9$. Furthermore, within the detection limits of the instrument, no other extraneous elements were detected.

Results and Discussion

Room-Temperature Structures. Small hexagonal blocks and double hexagonal pyramid crystals of $Ba_3MRu_2O_9$ (M = Li, Na) were isolated from molten hydroxide fluxes in which the flux acted as both melt and reactant. Figure 1 is an ESEM image of $Ba_3NaRu_2O_9$, showing the interesting hexagonal pyramid type morphology of the crystals. Some of the crystals, in fact, are

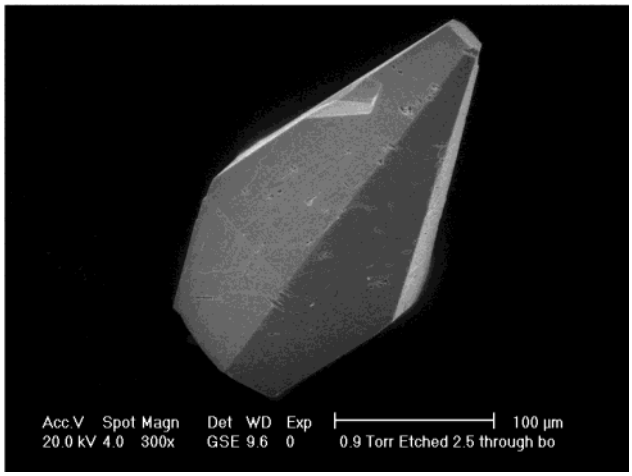

Figure 1. ESEM image of a flux-grown single crystal of $Ba_3NaRu_2O_9$.

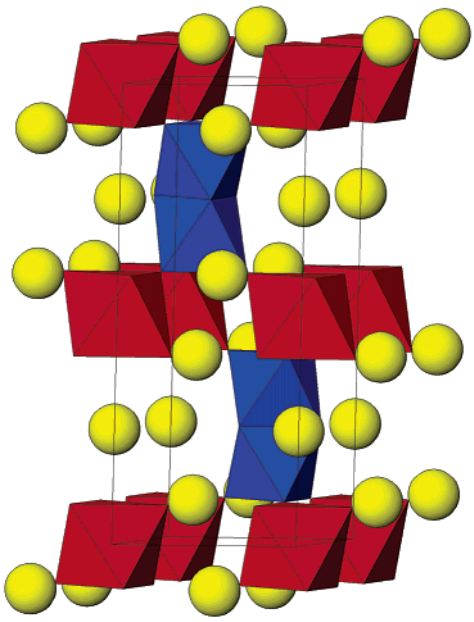

Figure 2. Approximate [110] view of the structure of $Ba_3MRu_2O_9$ (M = Li, Na) consisting of blue RuO_6 face-sharing bi-octahedra cornered shared to red MO_6 (M = Li, Na) octahedra singles. Barium cations are shown as yellow spheres.

double pyramids where the two hexagonal pyramids share a common base. The sodium and lithium ruthenate crystals measured on average 0.1−0.2 mm in length. The ESEM verified the presence of barium, sodium, ruthenium, and oxygen for $Ba_3NaRu_2O_9$ and barium, ruthenium, and oxygen for $Ba_3LiRu_2O_9$; however, lithium was not observed because it is below the detection limits of the instrument. In both cases, no additional extraneous elements were identified within the detection limits of the instrument.

The room-temperature structures of $Ba_3MRu_2O_9$ (M = Li, Na) crystallize in the 6H-$BaTiO_3$ structure type[36] in the space group $P6_3/mmc$. An approximate [110] view of the structure is shown in Figure 2. The structure consists of face-sharing Ru_2O_9 bi-octahedra, which in turn share six vertexes with six AO_6 (A = Li, Na) octahedra. The barium cations are located in cuboctahedral 12-fold coordination sites. The Ru−O bond

(36) Burbank, R. D.; Evans, H. T. *Acta Crystallogr.* **1948**, *1*, 330.

Table 7. Selected Interatmic Distances

atom–atom	distance (Å)		atom–atom	distance (Å)	
		$Ba_3LiRu_2O_9$			
Li(1)−O(2)	2.123(3)	(×6)	Ru(1)−O(2)	1.852(3)	(×3)
Ru(1)−Ru(1)	2.768(1)	(×1)	Ru(1)−O(1)	2.039(3)	(×3)
		$Ba_3NaRu_2O_9$ − Room-Temperature Structure			
Na(1)−O(1)	2.227(3)	(×6)	Ru(1)−O(1)	1.842(3)	(×3)
Ru(1)−Ru(1)	2.7482(9)	(×1)	Ru(1)−O(2)	2.046(3)	(×3)
		$Ba_3NaRu_2O_9$ − Low-Temperature Structure			
Na(1)−O(11)	2.158(12)	(×2)	Ru(2)−O(23)	1.852(15)	(×1)
Na(1)−O(21)	2.239(10)	(×2)	Ru(2)−O(22)	2.003(14)	(×1)
Na(1)−O(31)	2.284(8)	(×2)	Ru(2)−O(24)	2.078(10)	(×2)
Na(2)−O(34)	2.238(8)	(×4)	Ru(3)−O(34)	1.794(8)	(×1)
Na(2)−O(23)	2.295(13)	(×2)	Ru(3)−O(35)	1.814(8)	(×1)
Na(3)−O(14)	2.245(10)	(×2)	Ru(3)−O(31)	1.847(7)	(×1)
Na(3)−O(35)	2.298(8)	(×4)	Ru(3)−O(33)	2.042(17)	(×1)
Ru(1)−O(14)	1.910(10)	(×1)	Ru(3)−O(36)	2.048(7)	(×1)
Ru(1)−O(11)	1.932(13)	(×2)	Ru(3)−O(32)	2.050(14)	(×1)
Ru(1)−O(13)	2.047(12)	(×2)	Ru(1)−Ru(1)	2.614(3)	(×1)
Ru(1)−O(12)	2.090(20)	(×1)	Ru(2)−Ru(2)	2.653(4)	(×1)
Ru(2)−O(21)	1.831(10)	(×2)	Ru(3)−Ru(3)	2.848(1)	(×1)

distances range from 1.842 to 2.046 Å and agree well with those reported in the literature for other RuO_6 octahedra in triple perovskite structures.[12,16,37] Likewise, the observed M−O distances for the lithium and sodium octahedra at 2.123(3) and 2.227(3) Å, respectively, agree with other MO_6 octahedra in perovskite-related structures that we have measured.[4] The Ru−Ru distances at 2.768(1) and 2.7482(9) Å for the lithium- and sodium-containing ruthenates, respectively, are at least 0.1 Å longer as compared to typical distances for other ruthenium triple perovskites (vide infra). All crystallographic data and atomic positions are listed in Tables 1 and 3 for $Ba_3LiRu_2O_9$ and Tables 2 and 4 for $Ba_3NaRu_2O_9$. Selected interatomic distances are listed in Table 7.

While there are many known examples of 6H-perovskite (triple perovskite) structures with the general formula $Ba_3MRu_2O_9$, including $Ba_3MRu_2O_9$ (M = Ni, Co, Zn),[11,38] $Ba_3NdRu_2O_9$,[16] $Ba_3CeRu_2O_9$,[39] $Ba_3LnRu_2O_9$ (Ln = Ce, Pr, Tb),[12] $Ba_3MRu_2O_9$ (M = Mg, Ca, Cd, Sr),[15] $Ba_3MRu_2O_9$ (M = Y, Gd, Yb),[40] $Ba_3InRu_2O_9$,[41] and $Ba_3CuRu_2O_9$,[37] none contain ruthenium in a formal oxidation state of +6. In most of these $Ba_3MRu_2O_9$ examples, the M cation is typically di-, tri-, or tetravalent, effecting formal oxidation states for ruthenium of +5 and +4, respectively. In some instances where M = rare earth and hence has an odd valence, a mixed valency is forced upon the ruthenium for charge balance. This is the case for neodymium, oxidation state of +3, where the average oxidation state of ruthenium is +4.5[16] as well as for other +3 lanthanides, Sm, Dy, and Er, that lead to mixed Ru +4/+5 systems.[39] This is also the case for our new ruthenates, where the +1 oxidation state of the alkali metal cation effects an unusually high +5/+6 mixed valency for ruthenium. It is important to point out that in the *room-temperature* triple perovskite structure of $Ba_3MRu_2O_9$ (M = Li, Na), the Ru(V) and Ru(VI) must be disordered, as there is only one unique crystallographic site for ruthenium. This fact becomes more important as we discuss the low-temperature structure (vide infra). $Ba_3MRu_2O_9$ (M = Li, Na) represent the first examples of ordered ruthenium triple perovskites containing an alkali metal and, furthermore, two of only a few oxide compounds reported to contain ruthenium in as high of an oxidation state as +6.[14] Quadruple perovskites containing alkali metals and Ru(V) such as $Ba_4NaRu_3O_{12}$ as well as one disordered triple perovskite containing an alkali metal and Ru(V) $Ba_4LiRu_3O_{12}$ (equivalent to $Ba_3Li_{3/4}Ru_{9/4}O_9$) have been reported by Battle et al.[13] The materials reported in this paper represent an extension on the work by Battle and co-workers by expanding the known ruthenium oxidation states in triple perovskites to mixed +5 and +6.

To support the high formal oxidation state (V/VI) of ruthenium in Ba_3MRuO_6 (M = Li, Na), we compared the Ru−Ru distances and the Ru−O distances in the bi-octahedra with other fully structurally characterized $Ba_3MRu_2O_9$ triple perovskites. A plot of Ru−Ru distance as a function of the average formal ruthenium oxidation state is shown in Figure 3a. Clearly, as the average formal oxidation state increases, the Ru−Ru bond length increases with a tight clustering of distances for each average oxidation state. The Ru−Ru distances of 2.768(1) and 2.7482(9) Å for the lithium- and sodium-containing ruthenates, respectively, are on the order 0.1 Å longer as compared to the formally +5 ruthenium systems, which in turn are approximately 0.1 Å longer than the +4.5 ruthenium systems. The reason for this increase in the Ru−Ru separation with increasing formal oxidation state is undoubtedly due to increased Ru−Ru repulsion, in other words, a primarily Coulombic effect. Hence, the long Ru−Ru separation in $Ba_3LiRu_2O_9$ and $Ba_3NaRu_2O_9$ is consistent with their high formal oxidation states.

Accompanying this increase in the Ru−Ru separation should be a decrease in the Ru−O distances, as this bond is expected to shorten with increasing metal oxidation state. This trend is shown in Figure 3b, where the Ru−O distances (plotted for the outer oxygens only) in fully structurally characterized $Ba_3MRu_2O_9$ triple perovskites are plotted against the average formal Ru oxidation state. Here we see the expected trend of a decrease in the bond length with increasing oxidation state. Again, the distances are clustered for each oxidation state, but not as tightly as for the Ru−Ru distances. One reason for this scatter is the asymmetrical shape of the bi-octahedra. While the Ru−O distances for the inner three oxygens stay approximately constant at 2.00−2.02 Å for *all* of the $Ba_3MRu_2O_9$ oxides, the Ru−O distances to the six outer oxygens change systematically with the ruthenium oxidation state. To achieve these constant Ru−O distances of the inner oxygens with increasing oxidation state, while also satisfying the need for longer Ru−Ru separation, the oxygens in the shared face move in, increasing the Ru−O−Ru angle. Clearly, however, the trend of Ru−O distance with oxidation state supports our assignment of the V/VI formal oxidation states in our new oxides.

This trend appears general for structures containing Ru_2O_9 bi-octahedra, as the Ru−Ru and Ru−O distances of the quadruple perovskite $Ba_4NaRu_3O_{12}$ reported by Battle[13] also fit into the Ru−Ru and Ru−O distance plots shown in Figure 3. In $Ba_4NaRu_3O_{12}$, ruthenium is +5 with a Ru−Ru distance of 2.66(2) Å, which corresponds well to the average Ru−Ru separation of 2.67(2) Å for the +5 oxidation state, as shown in Figure 3a. Concomitantly, the Ru−O distances are 1.88(1) and 1.95(2) Å, which again agree with those plotted in Figure 3b

(37) Rijssenbeek, J. T.; Huang, Q.; Erwin, R. W.; Zandbergen, H. W.; Cava, R. J. *J. Solid State Chem.* **1999**, *146*, 65.
(38) Donohue, P. C.; Katz, L.; Ward, R. *Inorg. Chem.* **1966**, *5*, 339.
(39) Müller-Buschbaum, H.; Mertens, B. *Z. Naturforsch., B: Chem. Sci.* **1996**, *51*, 79.
(40) Rath, M.; Müller-Buschbaum, H. *J. Alloys Compd.* **1994**, *210*, 119.
(41) Schaller, H.-U.; Kemmler-Sack, S. *Z. Anorg. Allg. Chem.* **1981**, *473*, 178.

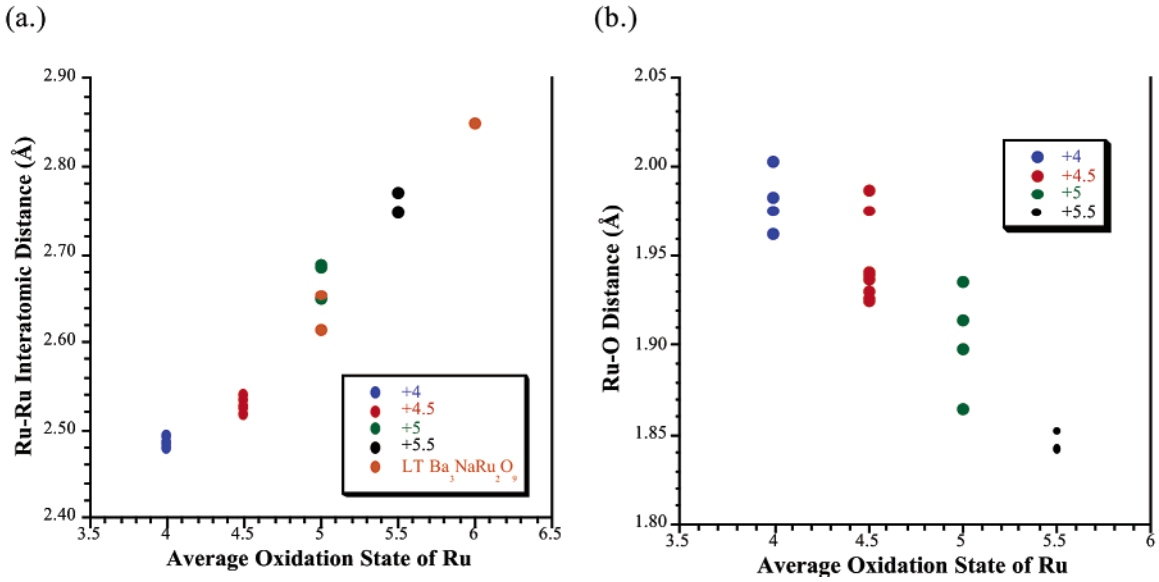

Figure 3. (a) Ru−Ru interatomic distance within the face-sharing bi-octahedra of $Ba_3MRu_2O_9$ as a function of the average formal oxidation state of Ru. (b) Ru−O distance for the outer six oxygens of the bi-octahedra as a function of the average formal oxidation state of Ru. The Ru−O distance for the inner three oxygens is approximately constant for all of the compounds plotted at 2.00−2.02 Å. Only compounds solved in the space group $P6_3/mmc$ with no site mixing were considered. Compounds used to generate the plot include $Ba_3MRu_2O_9$, where M = Ce,[12,39] Pr,[12] Tb,[12] for Ru(+4) − blue; M = Y,[40] Gd,[40] Yb,[40] Sm,[39] Dy,[39] Er,[39] Nd,[16] In,[37] for Ru(+4.5) − red; M = Co,[37] Ni,[37] Zn,[11] Ca,[15,42] for Ru(+5) − green; M = Li, Na from the present paper for Ru(+5.5) − black. Additionally, the three Ru−Ru interatomic distances of the low-temperature structure of $Ba_3NaRu_2O_9$ (orange) have been plotted in (a) to show the expected oxidation states for the three ruthenium sites on the basis of their Ru−Ru distances. The low-temperature Ru−O distances were not included in (b), as the low-temperature structure does not have the same sets of Ru−O distances observed in the high-temperature structure (three long and three short) due to the much lower site symmetry (four, four, and six unique Ru−O distances for Ru(1), Ru(2), and Ru(3), respectively).

for Ru(V) with an average of 1.90(2) Å. An analogous comparison cannot easily be made for $Ba_4LiRu_3O_{12}$ where there is site mixing and both Ru and Li are found in the bi-octahedra.

Low-Temperature Structure of $Ba_3NaRu_2O_9$. At room temperature and down to approximately 225 K, $Ba_3NaRu_2O_9$ exists as a normal triple perovskite with a primitive hexagonal lattice, space group $P6_3/mmc$, with a = 5.8729(2) Å and c = 14.4676(7) Å. The structure contains one crystallographically unique ruthenium atom, which generates equivalent Ru_2O_9 face-sharing bi-octahedra throughout the structure with Ru−Ru distances of 2.7482(9) Å. Cooling below the transition temperature is accompanied by an apparent doubling of the hexagonal a and b axes and a slight broadening of the reflection profiles. All reflections can still be indexed to a primitive hexagonal lattice, with $a \approx 11.73$ and $c \approx 14.49$. Although the lattice is still metrically hexagonal, the internal symmetry has been broken by the formation of three inequivalent Ru_2O_9 bi-octahedra, with two short and one long Ru−Ru distances (Ru1−Ru1 = 2.614(3) Å; Ru2−Ru2 = 2.653(4) Å; Ru3−Ru3 = 2.848(1) Å). The resulting C-centered orthorhombic cell (space group $Cmcm$, a = 11.7282(8) Å, b = 20.3541(13) Å, c = 14.4856(10) Å) is in fact the orthohexagonal cell (Figure 4a) of the $2a \times 2b$ primitive hexagonal pseudocell ($a \approx 11.73$ Å, $c \approx 14.49$ Å). This transformation between the high-temperature $P6_3/mmc$ phase and its maximal nonisomorphic subgroup $Cmcm$ low-temperature phase is of the t3 (translationengleiche, index 3) type and as such is necessarily accompanied by three-fold twinning ("trilling"). The twin element is the three-fold axis of rotation, lost during the reduction in symmetry. The twin element simply relates the three nonequivalent orthohexagonal cells (see Figure 4b) to one another. In matrix notation, the twin law for

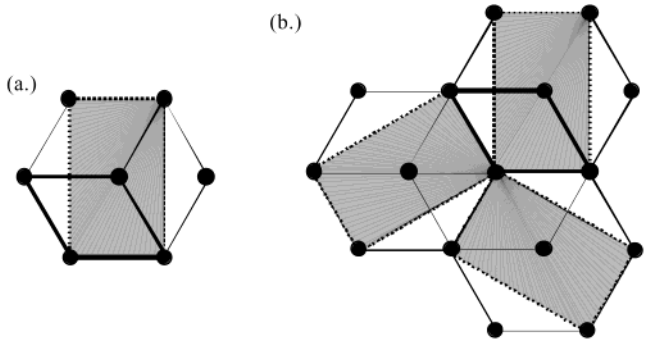

Figure 4. (a) The three equivalent hexagonal cells are outlined in black. The C-centered orthohexagonal cell (shaded gray) is equivalent to the boldfaced hexagonal cell, where $a_{ortho} = a_{hex}$, $b_{ortho} = \sqrt{3}b_{hex}$, and $c_{ortho} = c_{hex}$. (b) The three twin domains of the low-temperature form of $Ba_3NaRu_2O_9$ (shaded gray), mutually related by a 120° rotation.

a three-fold axis on orthorhombic axes is expressed as

$$\begin{bmatrix} -0.5 & 0.5 & 0 \\ -1.5 & -0.5 & 0 \\ 0 & 0 & 1 \end{bmatrix}$$

The approximate fractions of the three twin domains, as determined by refinement of the scale factors for each domain using SHELX, are $k1 = 0.401$, $k2 = 0.300$, $k3 = 0.299$, that is, close to a perfectly "trilled" crystal ($k1 = k2 = k3 = 1/3$). The crystallographic data and atomic positions for the low-temperature structure are compiled in Tables 5 and 6, respectively. This structure transition is completely reversible and, aside from the initial peak broadening due to the trilling, causes no changes in the crystal.

Although structural transitions have been observed in other triple perovskites, such as $Ba_3CoRu_2O_9$[11] and $Ba_3NdRu_2O_9$,[16]

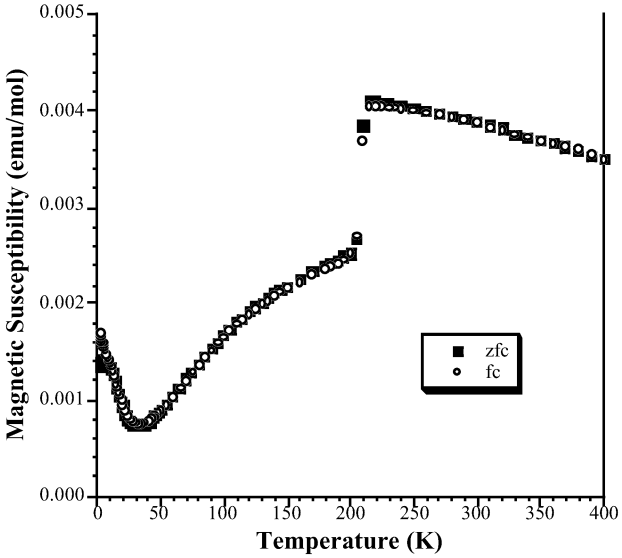

Figure 5. Temperature dependence of the zero field cooled (zfc; ■) and field cooled (fc; ○) magnetic susceptibility of loose crystals of $Ba_3NaRu_2O_9$ at an applied field of 20 kG.

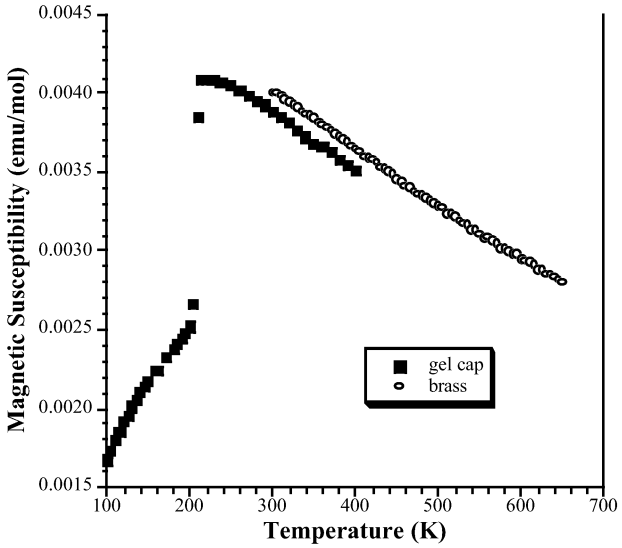

Figure 6. High temperature dependence of the magnetic susceptibility of loose crystals of $Ba_3NaRu_2O_9$ at an applied field of 20 kG measured in a straw−gel cap assembly (■) and the high-temperature brass sample holder (○).

this exact structure solution of the trilled low-temperature form of $Ba_3NaRu_2O_9$ is, to the best of our knowledge, the first reported example. In the case of $Ba_3CoRu_2O_9$ and $Ba_3NdRu_2O_9$, which were solved in the space groups *Cmcm* and *C*2/*c*, respectively, both structures retained only one unique Ru site, generating only one Ru−Ru distance, close to those observed in the room-temperature structures. Consequently, our structure solution represents the first crystallographic study to detail the formation of the three inequivalent Ru_2O_9 bi-octahedra with three Ru−Ru separations associated with this phase transition. In fact, the single-crystal structure solution of the high- and low-temperature forms of $Ba_3NaRu_2O_9$ represents the first example of an exact solution for the hexagonal to orthohexagonal (orthorhombic) trilling process for perovskites in general.

Low-Temperature Structure of $Ba_3LiRu_2O_9$. Perhaps equally interesting is the fact that the lithium analogue does not have a structural transition down to the lowest temperature measured (100 K) and that there is no compelling indication in the magnetic data (vide infra) that such a structural transition exists at lower temperatures. The lithium and the sodium ruthenates are isostructural at room temperature where they differ only slightly in their lattice parameters, $a = 5.7820(2)$ Å, $c = 14.1490(8)$ Å versus $a = 5.8729(2)$ Å, $c = 14.4676(7)$ Å for the lithium and sodium case, respectively. This difference, however, is concentrated in the sizes of the LiO_6 (Li−O 2.123(3) Å) and NaO_6 (Na−O 2.227(3) Å) octahedra rather than in the Ru_2O_9 bi-octahedra, which have virtually the same bond lengths (Li: Ru−O, 1.852(3) and 2.039(3) Å; Na: Ru−O, 1.842(3) and 2.046(3) Å) in both compounds. One would have to speculate that this size difference is just enough to facilitate the transition to occur in the sodium but not in the lithium-containing ruthenate.

Magnetism. The temperature dependence of the magnetic susceptibility for $Ba_3NaRu_2O_9$, measured in an applied field of 20 kG, is shown in Figure 5. Most notable about the temperature sweep is the precipitous drop in the susceptibility at 210 K, occurring over a span of only 10 K, followed by a gradual decrease in the susceptibility to the minimum value at 33 K. The susceptibility then increases with the zero field cooled (zfc) and field cooled (fc) data diverging at low temperatures. It is important to point out that at higher temperatures ($T > 50$ K), the zfc and fc data overlay completely and that the precipitous drop at 210 K is completely reversible in nature and cycling through the transition several times leaves the onset and width of the transition unchanged. Furthermore, additional batches of single crystals were prepared to investigate the reproducibility of this susceptibility drop, which correlates with the structural transition described above. All batches displayed the same magnetic behavior with the susceptibility drop at 210 K.

To extract a magnetic moment from the data, the high-temperature portion of the susceptibility plot was investigated. As it is desirable to use data of a temperature regime that starts at no less than 2× any ordering temperature, it was necessary to measure the susceptibility to higher temperatures. This was achieved using a Quantum Design oven attachment in which the sample was contained within a machined brass sample holder. The high temperature dependence of the susceptibility is shown in Figure 6, with an overlay of the low-temperature data, which were collected in a straw−gel cap assembly. The slopes of the two data traces are noticeably the same; however, there is some offset between the two data sets, which is attributed to a combination of the differences in the materials, shape, and masses of the sample holders. Fitting the high-temperature susceptibility data ($400 \leq T \leq 650$) of $Ba_3NaRu_2O_9$ to the Curie−Weiss Law yields an effective moment of 4.89 μ_B with $\theta = -429$ K. It should be noted that there is a large uncertainty in the θ value due to the shift of the data trace collected at high temperature, and thus this value should be viewed as qualitative rather than representing a quantitative result; nonetheless, irrespective of the exact θ value, the very large negative Weiss constant indicates significant antiferromagnetic correlations in this material. This is consistent with the precipitous drop in the susceptibility at 210 K and the subsequent decrease in the magnetic susceptibility due to antiferromagnetic correlations. Whether in fact these antiferromagnetic correlations cause the structural transition and concomitant magnetic transition, or whether a size mismatch

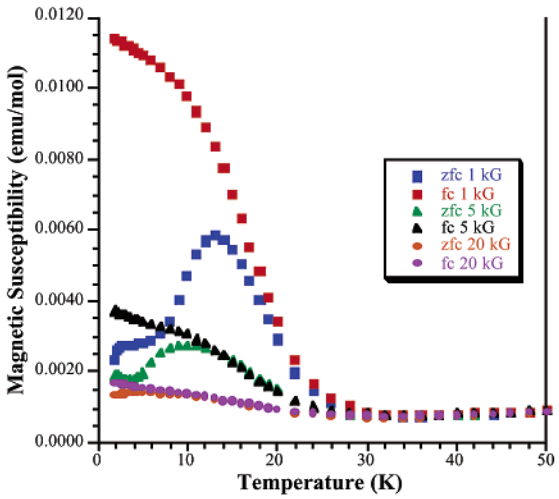

Figure 7. Low temperature dependence of the magnetic susceptibility of loose crystals of $Ba_3NaRu_2O_9$ at applied fields of 1 kG (zfc − blue squares; fc − red squares), 5 kG (zfc − green triangles; fc − black triangles), and 20 kG (zfc − orange circles; fc − purple circles).

between the sodium and ruthenium cations triggers the structural transition and thus effects the magnetic changes, is a question that remains under investigation.

The field dependence of the susceptibility at low temperatures is shown in Figure 7. The decrease in susceptibility beginning at 210 K is followed by a second magnetic transition at 33 K, after which the susceptibility ceases to be field-independent. The fc and zfc data no longer overlay, and, depending on the applied field used for the measurements, a third magnetic transition is observed at 15 K. This transition is most noticeable in the lowest applied field used and is completely suppressed in fields exceeding 20 kG. Only in the zfc data are antiferromagnetic correlations prominent, while under fc conditions a ferromagnetic-like increase is observed. This is reminiscent of a spin frustration and is possibly due to the presence of the three crystallographically unique ruthenium sites with competing magnetic interactions in the low-temperature structure. This ferromagnetic-like increase can be explained by the failure of the spins to achieve antiferromagnetic alignment in an applied field when the antiferromagnetic correlations are weak.

The magnetic behavior of this material can be divided into two unique regimes that are separated by a structural transition at 225 K. In the high-temperature regime, the magnetic susceptibility arises from the presence of ruthenium on the single crystallographic site, where charge balance dictates that $Ba_3NaRu_2O_9$ must contain one Ru(V) and one Ru(VI), given that all other elements are fixed valent. Because there is only one unique crystallographic site in the room-temperature structure of $Ba_3NaRu_2O_9$, the Ru(V) and Ru(VI) must be disordered throughout the structure. On the basis of these oxidation states and the octahedral coordination environments, the theoretical spin-only moment for this compound is 4.79 μ_B, which agrees well with the experimentally determined value of 4.89 μ_B.

In the low-temperature region, on the other hand, the susceptibility results from the presence and interactions of ruthenium cations on three distinct crystallographic sites that generate three distinct face-sharing ruthenium bi-octahedra. These three unique Ru sites are generated by the reduction of symmetry and the loss of the three-fold axis. Because of the site multiplicity, the number of generated Ru3 sites equals the combined number of generated Ru1 and Ru2 sites. Thus, the numerical equality of [Ru3] and [Ru2 + Ru1] enables all of the Ru(VI) cations to be in one set of bi-octahedra and all of the Ru(V) cations to be in the other two pairs (or vice versa). Consequently, one must seriously consider the possibility that the ruthenium cations might be charge ordered at low temperature and that this pairing-up of Ru(V)−Ru(V) and Ru(VI)−Ru(VI) might be the driving force for the structural transition. To assess whether charge ordering occurred during the structural transition, it is necessary to compare the Ru−Ru distances and the Ru−O distances in the bi-octahedra of this low-temperature structure with those found in other fully structurally characterized $Ba_3MRu_2O_9$ triple perovskites.

On inspection one finds that, while the average Ru−O bond distances in the three bi-octahedra are very similar, the Ru−Ru interatomic distances are quite different, and two pairs have short (2.614(3), 2.653(4) Å) and one pair has a long (2.848(1) Å) Ru−Ru distance. These three Ru−Ru distances fit nicely into the trend shown in Figure 3, a plot of the Ru−Ru distances as a function of average oxidation state, where these three distances are included using a distinct symbol. Clearly, the two short distances of 2.614(3) and 2.653(4) Å fall into the group of distances found for Ru(V)−Ru(V) pairs, that average around 2.67 Å. The long Ru−Ru distance of 2.848(1) Å, on the other hand, is significantly longer than the distances for even the Ru(V)−Ru(VI) pairs found in $Ba_3LiRu_2O_9$ and $Ba_3NaRu_2O_9$ and needs to be placed into its own group. There are no literature data for Ru(VI)−Ru(VI) pairs; however, on the basis of the trend started by the lower oxidation states (+4, +4.5, +5, +5.5), this distance of 2.848(1), approximately 0.1 Å longer than the one for Ru(+5.5), is consistent with oxidation states of +6 for this ruthenium pair.

This analysis of the Ru−Ru distances in the low-temperature structure strongly supports the assertion that charge ordering took place during the phase transition, implying that the Ru(V) and Ru(VI) cations that are disordered on a single crystallographic site in the high-temperature structure are crystallographically ordered in the low-temperature structure. This charge ordering is also consistent with the decrease in the susceptibility observed below the structural transition, where we might expect antiferromagnetic coupling between the ruthenium cations within each bi-octahedra. By contrast, bi-octahedra containing mixed Ru(V)/Ru(VI) would result in uncompensated spins that should lead to an increase in the susceptibility, which is not consistent with the observed data.

The original preparation of $Ba_3LiRu_2O_9$ was not phase pure, but contained small amounts of $Ba_7Li_3Ru_4O_{20}$,[43] a new perovskite-related oxide with a large c-parameter, as an impurity that could not be physically separated. However, by changing the reaction conditions to a "wet" melt of LiOH/KOH, a phase pure sample could be synthesized. The magnetic susceptibility as a function of temperature at an applied field of 20 kG was collected on this "wet" sample preparation, as shown in Figure 8. The fc data of the susceptibility (2 K $\leq T \leq$ 400 K) have been omitted for clarity as the zfc and fc completely overlay. At 140 K, there is a slight drop in the susceptibility, however, neither as large nor as drastic as that seen for $Ba_3NaRu_2O_9$. At lower temperatures, the susceptibility continues to slightly

(42) Wilkens, J.; Müller-Buschbaum, H. *J. Alloys Compd.* **1991**, *177*, L31.
(43) Stitzer, K. E.; Smith, M. D.; zur Loye, H.-C., in preparation.

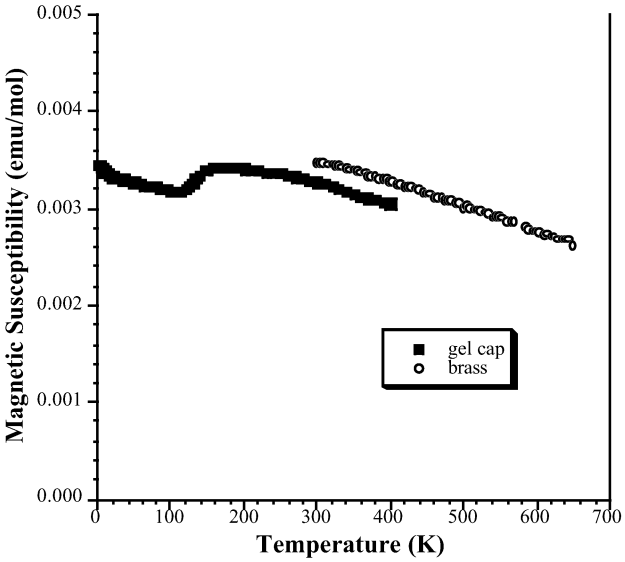

Figure 8. Temperature dependence of the magnetic susceptibility of loose crystals of $Ba_3LiRu_2O_9$ measured in a straw−gel cap assembly (■) and the high-temperature brass sample holder (○) at an applied field of 20 kG.

increase with no apparent downturn to the lowest measured temperature of 2 K. The drop at 140 K does not correlate to a structural transition, which was crystallographically tested down to 100 K. It might be interesting, though, to investigate the temperature regime below 100 K for the existence of a structural transition. Again, to obtain an estimate of the magnetic moment for this sample, the susceptibility was collected at higher temperatures, to be sufficiently away from the drop at 140 K, using the Quantum Design oven attachment with the brass sample holder. The high-temperature data, as shown in Figure 8, have a slight offset from the low-temperature straw−gel cap assembly similar to the $Ba_3NaRu_2O_9$ data. Fitting these data ($400\ K \leq T \leq 650\ K$) to the Curie−Weiss Law yields an effective moment of 5.18 μ_B with $\theta = -634$ K. Again, these values should only be considered qualitative in nature, but the moment is close to the theoretical spin-only moment of 4.79 μ_B, and the very large Weiss constant would indicate significant antiferromagnetic correlations.

Summary

Two new Ru(V/VI) mixed-valent oxides were synthesized in single-crystal form and structurally characterized. The growth of these oxides from molten hydroxide fluxes further establishes these melts as a successful solvent system for the preparation of oxide structures containing noble metals in unusually high oxidation states. $Ba_3LiRu_2O_9$ and $Ba_3NaRu_2O_9$ form in the triple perovskite structure, and $Ba_3NaRu_2O_9$ undergoes a structural phase transition at 225 K that is accompanied by a precipitous drop in the magnetic susceptibility that is consistent with a charge ordering process. These oxides are the first structurally characterized triple perovskites containing ruthenium in the +6 oxidation state.

Acknowledgment. Financial support from the National Science Foundation through Grant DMR:0134156 is gratefully acknowledged. We also thank Dr. Jacques Darriet and Dr. Ahmed El Abed of the ICMCB-CNRS for many helpful discussions.

Supporting Information Available: X-ray crystallographic files are available in CIF format: tables of crystal data and refinement information as well as of fractional atomic coordinates and displacement factors of the atoms. This material is available free of charge via the Internet at http://pubs.acs.org.

JA0271781